

The parametric study of an electrical submersible pump rotary gas separator under two-phase flow condition

Authors

Saba Darbani^a
Alireza Riasi^{a*}
Amir Nejat^a

^a School of Mechanical Engineering,
College of Engineering, University of
Tehran, P.O. Box 11155-4563, Tehran,
Iran

ABSTRACT

The performance of the electric submersible pump (ESP) significantly affected by Gas Void Fraction (GVF). Thus, using of a Rotary Gas Separator (RGS) is a suitable solution for this issue. The performance of the RGS is function of different parameters such as geometry of impeller, rotating speed, boundary conditions, media viscosity and GVF. In this study, the influences of GVF, viscosity, and flow rate on vortex and paddle wheel gas separator have been studied. For this purpose, commercial CFD software has been implemented. As results show, paddle wheel geometry is more efficient in comparison to the vortex gas separator in same conditions. Nevertheless, low efficient region occurs in high flow rates. In other words in flow rates higher than 1000 bpd efficiency of separator is lower than 50% which means that only the natural separation occurs in RGS equipment. Paddle wheel separator is more sensitive to GVF increase in high viscosities and the dropdown of efficiency in viscosity of 10 cp is about 20 in percent. The opposite happens with vortex gas separator in which the separation efficiency is more sensitive to increase of GVF of liquid stream in lower viscosities.

Article history:

Received : 15 November 2014

Accepted : 8 December 2014

Keywords: Rotary Gas Separator, Electric Submersible Pump (ESP), Paddle Wheel Gas Separator, Vortex Gas Separator.

1. Introduction

Oil wells at the beginning of their existence could lift oil to the surface naturally. This actually means that the total pressure of oil well is enough to overcome all the pressure loss during liquid flow. As the oil well gets old, the bottom hole pressure of the well decreases and the problem of oil recovery arises accordingly.

There are different methods used in oil recovery from underground resources and oil wells. When the well gets old and oil ceases to flow naturally to the surface, the secondary

recovery methods are employed. Secondary recovery methods include the injection of other fluids like water or gas into the oil media in order to aid the movement of bulk of oil to the surface. These secondary methods are devoid of the mixture of oil and injected fluid. When the secondary oil recovery methods become inefficient, the tertiary oil recovery methods are applied. In this step, various methods are used to increase the flow rate of oil to the well head. Hydrocarbon gases, nitrogen and polymers are mostly used as injected fluids into wells, in order to increase oil extraction. Typically, the first injected mass, which is an expensive material, is supported by the second and sometimes the third mass of injected fluids into the oil media in which the second and

*Corresponding author: Alireza Riasi
Address : Assistant Professor, School of Mechanical
Engineering, College of Engineering, University of Tehran,
P.O. Box 11155-4563, Tehran, Iran
E-mail address: ariasi@ut.ac.ir

third fluid masses are inexpensive and cheap materials. The use of submersible pumps for enhanced oil recovery is in this group.

Conversely, submersible pumps increase the pressure of the fluid in the well, so that the fluid's pressure can overcome all the pressure loss in its path. There are different classes of submersible pumps. Electrical Submersible Pump (ESP) is one of the important and commonly used ones among the different classes. These pumps consist of several stages of centrifugal pumps and earn its motivation power from the electric submersible motor. The key point is that, as the amount of free gas flow increases, the performance of these pumps significantly decrease. Thus, using RGS is a logical step for solving this issue [2].

Basically, all enhanced oil recovery methods have their own advantage based on the well's specifications, fluid properties and flow rate. However, in a specific situation different methods could be used and the decision depends on engineers. Fig.1 shows a comparison between these methods and the condition of their usage.

RGS is undertaken to separate gas and liquid phase using centrifugal force. Therefore, the geometry of RGS, which is constructed by an inducer and impeller, should be designed to provide adequate rotating velocity and less turbulence [3, 4].

The flow of media through the RGS is a 3D swirling flow which is extremely complex and its existence in two phases makes it extremely complex.

Hence, it is in fact difficult to analyze and predict the behavior of such a complex flow. In several studies, new numerical methods have been presented for analyzing the RGS [5,6]. Also, some studies used simplified solution to study the RGS [7].

However, the defining performance of function and the determination of the efficient working point of the RGS have been studied by several researchers. Alhanati has shown that each inducer has both high and low efficient regions. The transition between these two regions is considerably sharp. Thus, it is essential to determine the inducers regions [8]. Some other publications investigated the influence of the effect of rotating speed, inducer effect and impeller shape on RGS. Haruns introduced a model for analyzing the two phase media. Furthermore, this model was used to determine the accurate inducer head which is essential for detecting low and high efficiency [9]. In another study, an attempt was made to optimize the design of RGS by using inducer geometry and its head relation [9, 10, 12]. The media's parameters such as viscosity, density, GVF and surface tension on RGS were investigated. Lackner studied the effect of pressure, back flow rate, gas-liquid ratio, and rotational speed on the performance of RGSs [11]. Considering all above mentioned, it is obvious that the performance of the different type of impeller and inducers were not investigated in the same working condition. Focuses on the performance of popular RGS types such as paddle wheel

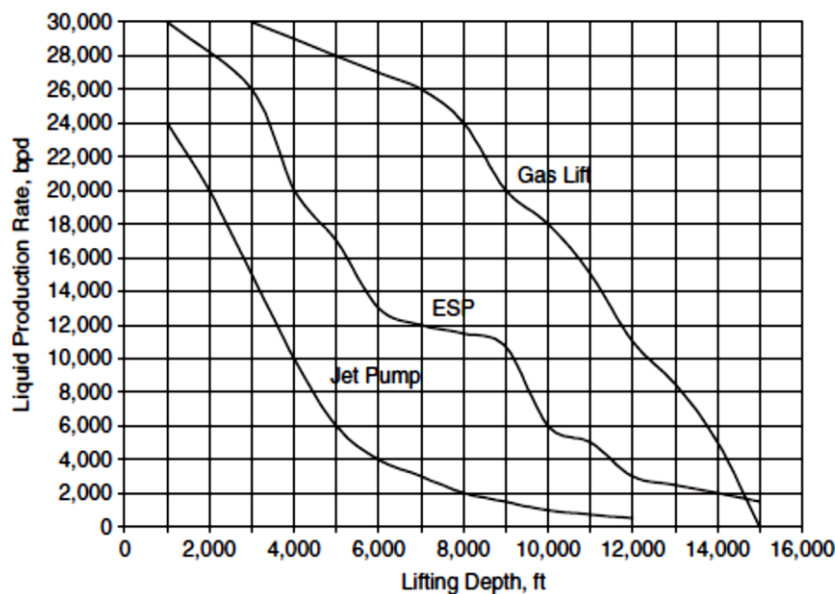


Fig. 1. Comparison of different methods of EOR based on oil liquid rate [3]

and vortex gas separator, are discussed further in this study. The results and the performance curve of the different types of RGS for different conditions of media have been presented and discussed in this study.

2.Theatrical Background

In order to gain knowledge of the separation process in an RGS, the Alhanati's model should be studied. This model was introduced by Alhanati in 1994 [13]. However, the model is a mathematical approach for anticipating the separation efficiency in submersible equipment.. Further, this model comprises of recursive stages. The separation process in an RGS installation primarily occurs in two distinct flow domains: in the RGS centrifugal chamber and within the tubing-casing annulus (called natural separation). The main importance of the natural separation is that it affects the actual amount of gas and liquid going into the separator. Also, the separation process in the centrifuge chamber affects the amount of gas and liquid expelled back into the annulus. Thus, the liquid that is expelled, as well as some of the gas recirculates back to the inlet port. Therefore, this process of recirculation of liquid and gas into the inlet is a hidden parameter in evaluating the RGS's efficiency.

Furthermore, the first stage of this model is to guess the flow rate of liquid and gas into the RGS and pump. Thereafter, the greater values are obtained for the gas flow rate into the RGS and pump by solving the two phase flow in annulus. In the third stage, the head generated by inducer (ΔP^+) is investigated. The gas outlet port discharge constant dictates the pressure drop (ΔP^-) across the port and is determined empirically as a result of the port's complex geometry, it should be noted that the inducer has to generate sufficient head to compensate for the pressure drop across the gas outlet port. Moreover, by solving the two phase flow equations inside the separation chamber, greater values are obtained for circulating flow rates. These steps should be done recursively until convergence occurs. For convergence, the head generated by inducer should be equal to the head loss across the outlet ports.

The basic definition and some:

components of an RGS equipment are as follows:

- Inducer

Inducer is a low head axial flow impeller with few blades, which is applied in the installation of RGS in order to provide sufficient head for the flow to overcome the outlet port pressure drops.

- Multiphase flow

In artificial lift in oil wells, the Gas Oil Ratio (GOR) is a commonly used parameter to determine the free gas amount flowing into the inlet ports.

- Separator chamber

In handling the higher amount of free gas in ESPs, there are stages with special impeller geometries that separates the gas and liquid via centrifugal force, thereby reducing the amount of gas in liquid stream for the subsequent pump stages and avoiding the pump gas lock.

- Separation efficiency

Separation efficiency is measured using mass balance on the liquid stream, comparing the amount of gas introduced into the inlet port of RGS to the amount of gas in liquid stream entering into the pump [14].

$$\eta_{sep} = (\dot{m}_{gin} - \dot{m}_{gout}) / \dot{m}_{gin} \quad (1)$$

where η_{sep} is separator efficiency.

\dot{m}_{gin} is the amount of mass flow of gas into the RGS.

\dot{m}_{gout} is the amount of mass flow of gas into the ESP.

3.Modeling and Numerical Simulation

The numerical simulation with CFD requires proper steps to obtain accurate results. Here, the CFD steps for the RGS internal flow simulation are defined:

- Geometry simulation

In all CFD analysis, the first step involves the definition of geometry in modeling software. The geometry of inducer, separator blades and crossovers has been generated using the commercial CAD software. All generated geometries were introduced into the CFD analysis software in IGS format. The geometry of separator and inducer and also the full RGS model are shown in Figs. 2, 3 and 4.

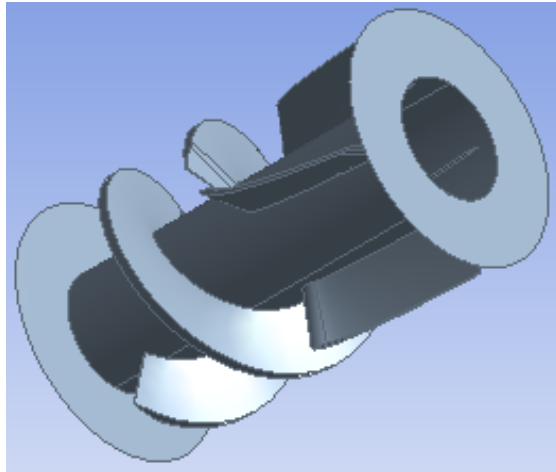


Fig. 2. Paddle wheel separator

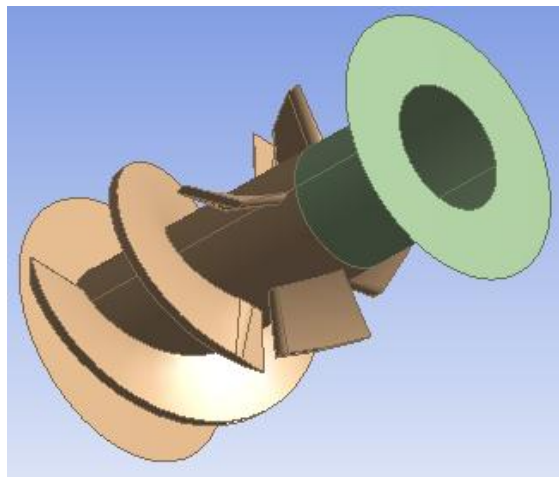


Fig. 3. Vortex separator

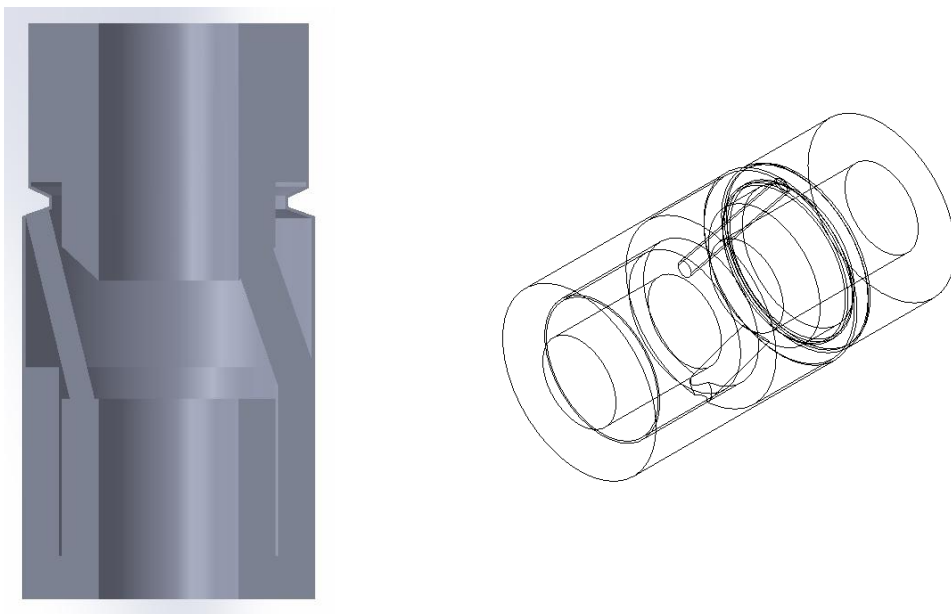


Fig. 4. Cross over

- Grid generation

Generated geometries have been introduced into commercial meshing program. The Patch conforming method is used for grid generation in these geometries. In places with high pressure gradient (boundary layers), inflation mesh is generated (Fig. 5). It is necessary to determine the influence of mesh size on solution and results. For this simulation, the torque value on separator and inducer blade is used as the parameter to evaluate four grids. The results show how the torque value trends to the asymptotic value when the number of nodes increases.

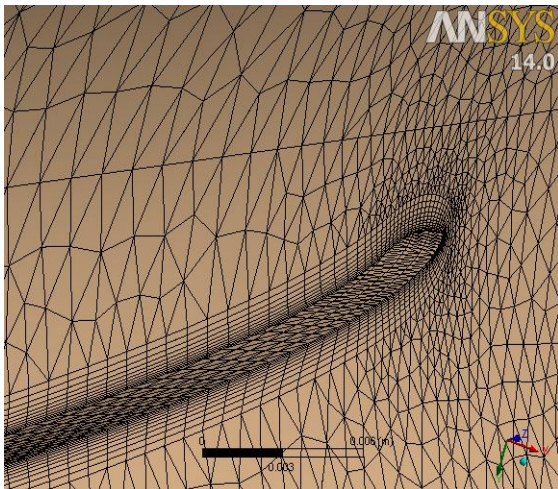
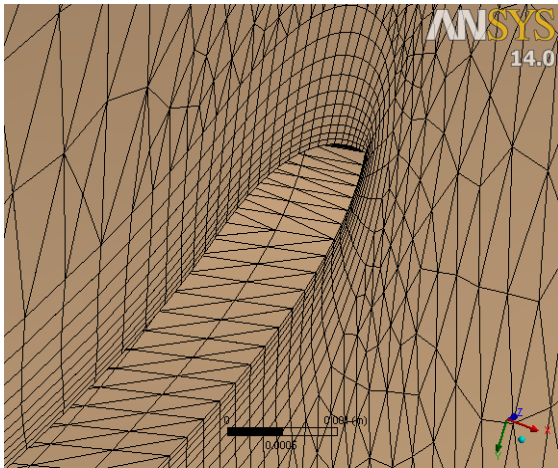


Fig. 5. Inflation layers

- Numerical method

The code in solving the Navier-Stokes equations using the finite volume method permit subdividing of the domain in several control volumes bounded by nodes. The Navier-Stokes equations consist of three main equations:

Mass conservation:

$$\frac{\partial \rho}{\partial t} + \frac{\partial}{\partial x_j} (\rho U_j) = 0 \quad (2)$$

Momentum conservation:

$$\frac{\partial}{\partial t} (\rho U_i) + \frac{\partial}{\partial x_j} (\rho U_j U_i) = -\frac{\partial P}{\partial x_j} + \frac{\partial}{\partial x_j} \left(\mu_{\epsilon jf} \left(\frac{\partial U_i}{\partial x_j} + \frac{\partial U_j}{\partial x_i} \right) \right) \quad (3)$$

Energy conservation:

$$\frac{\partial}{\partial t} (\rho \varphi) + \frac{\partial}{\partial x_j} (\rho U_j \varphi) = \frac{\partial}{\partial x_j} \left(\Gamma_{\epsilon jf} \left(\frac{\partial \varphi}{\partial x_j} \right) \right) + S_\varphi \quad (4)$$

The differential equations governing the phenomena are integrated for each control volume using the Gauss-Divergence theorem, Mass conservation integrated equation:

$$\frac{d}{dt} \int_V \rho dV + \int_S \rho U_j dn_j = 0 \quad (5)$$

Momentum conservation integrated equation:

$$\frac{d}{dt} \int_V \rho U_j dV + \int_S \rho U_j U_i dn_j = - \int_S P dn_j + \int_S \mu_{\epsilon jf} \left(\frac{\partial U_i}{\partial x_j} + \frac{\partial U_j}{\partial x_i} \right) dn_j + \int_V S_{U_j} dV$$

Energy conservation integrated equation:

$$\frac{d}{dt} \int_V \rho \varphi dV + \int_S \rho U_j \varphi dn_j = \int_S \Gamma_{\epsilon jf} \left(\frac{\partial \varphi}{\partial x_j} \right) dn_j + \int_V S_\varphi dV \quad (7)$$

Integration of each control volume leads a discrete equation that relates each variable in control volume with the variable of neighbor nodes, which guarantee the mass, energy and momentum conservation over the domain. An example of this discretization in the direction of the x axis is shown in Eq. 8:

$$a_p = \sum_{nb} a_{nb} u_{nb} + \sum p_f \widehat{e}_x A + S \quad (8)$$

By obtaining the pressure field and mass flux the above equation could be solved for each node and control volume.

- Multiphase flow

In this study, the particle model has been used to simulate the two-phase flow in the RGS. The particle model is subset of non-homogenous model and uses the Eulerian approach to simulate the multiphase flow.

In this model, one of the phases is considered as continuous phase (a) and the other as discrete phase (b).

- Turbulence model

The turbulence models, which are available for multiphase flow, are a generalized form of the single phase turbulence models. It is necessary to supply transfer terms between phases for κ and ε . For two-phase $\kappa - \varepsilon$ model, the turbulence viscosity is defined as shown in Eq.9:

$$\mu_{ta} = c_{\mu} \rho_a \left(\frac{k_a^2}{\varepsilon_a} \right) \quad (9)$$

Transport equation for κ (Eq.10) and ε (Eq.11) in multiphase flow is similar to the equations for this turbulence model in the single phase flow:

$$\begin{aligned} \frac{\partial}{\partial t} (r_{\alpha} \rho_{\alpha} k_{\alpha}) + \nabla \cdot \left(r_{\alpha} \left(\rho_{\alpha} U_{\alpha} k_{\alpha} - \left(\mu + \frac{\mu_{ta}}{\sigma_k} \right) \nabla k_{\alpha} \right) \right) \\ = r_{\alpha} (P_{\alpha} - \rho_{\alpha} \varepsilon_{\alpha}) + T_{\alpha\beta}^{(k)} \end{aligned} \quad (10)$$

$$\begin{aligned} \frac{\partial}{\partial t} (r_{\alpha} \rho_{\alpha} \varepsilon_{\alpha}) + \nabla \cdot \left(r_{\alpha} \rho_{\alpha} U_{\alpha} \varepsilon_{\alpha} - \left(\mu + \frac{\mu_{ta}}{\sigma_E} \right) \nabla \varepsilon_{\alpha} \right) \\ = \frac{r_{\alpha} \varepsilon_{\alpha}}{k_a} (C_{\varepsilon 1} P_{\alpha} - C_{\varepsilon 2} \rho_{\alpha} \varepsilon_{\alpha}) + T_{\alpha\beta}^{\varepsilon} \end{aligned} \quad (11)$$

The difference in two-phase turbulence model is in two additional terms of $T_{\alpha\beta}^{\varepsilon}$ and $T_{\alpha\beta}^{(k)}$ which shows transfer of κ and ε among between two phases.

Sato simulated the turbulence related to particles with improvement of Eddy viscosity equation for continuous phase:

$$\mu_{tc} = \mu_{ts} + \mu_{tp} \quad (12)$$

where μ_{ts} is indicates the Eddy viscosity from shear stress and μ_{tp} is the additional term from particles:

$$\mu_{tp} = 0.6 \rho_c r_d d_p |U_d - U_c| \quad (13)$$

This method is called the Sato Enhanced Viscosity Model.

- Boundary condition

The boundary conditions were fixed as:

- Inlet: Constant Total pressure applied in the rotation of axis direction and GVF.
- Liquid Outlet: constant mass flow
- Gas outlet: constant static pressure

- Wall (hub and blade): no-slip with velocity of 3500 rpm
- Wall (shroud): no-slip condition

After defining the above boundary conditions, the simulation starts running (Fig. 6).

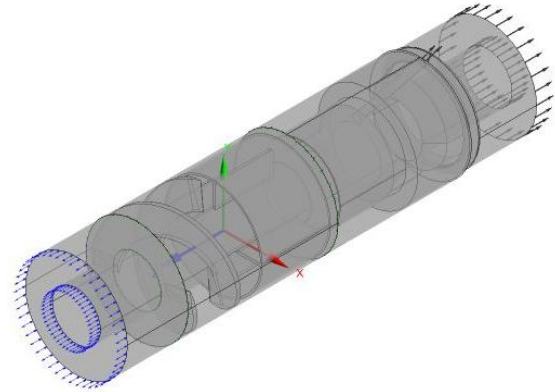


Fig. 6. Separator installation

4.Results and Discussion

In this study, the separation performance of two types of RGS were investigated under different flow conditions. Viscosity, volume fraction of gas flowing into RGS and the flow rate are the three parameters that have been changed in each simulation. The obtained results are indicated and discussed as follows.

- Grid independency

The number of elements which increases in order to examine the grid independency and torque, is considered as a variable that must be asymptote. The results of this study show the increase in the number of elements to 2,500,000 for the vortex gas separator and to 3,000,000 for the paddle wheel gas separator. However, the grid independency and the grid study for Vortex gas separator blades are shown in Figs. 7 and 8, respectively.

- The effect of viscosity and GVF on performance of each geometry

First of all, based on the Alhanati's model for the efficiency of RGS in low flow rates, the efficiency is high and is in the order of 90%, due to the fact that, in low flow rates, liquid stream stay longer in the separator chamber in order to complete the separation process. As a result, a sudden drop in the efficiency of RGS is observed in high flow rates. Based on the obtained results, this efficiency drop region occurs in higher flow rates in Paddle wheel separator rather than vortex gas separator.

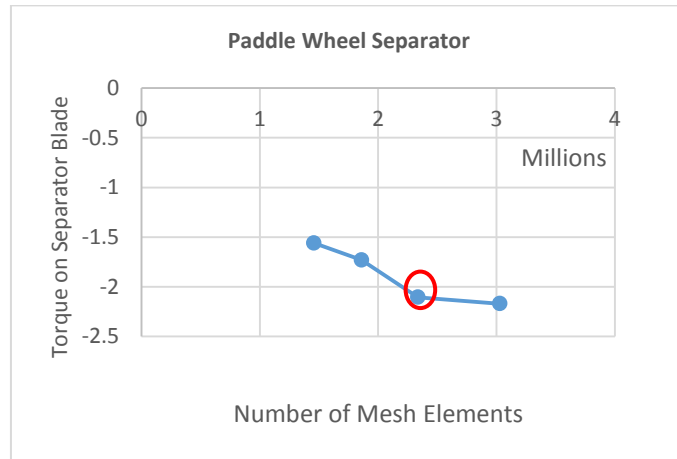


Fig. 7. Paddle wheel grid independency

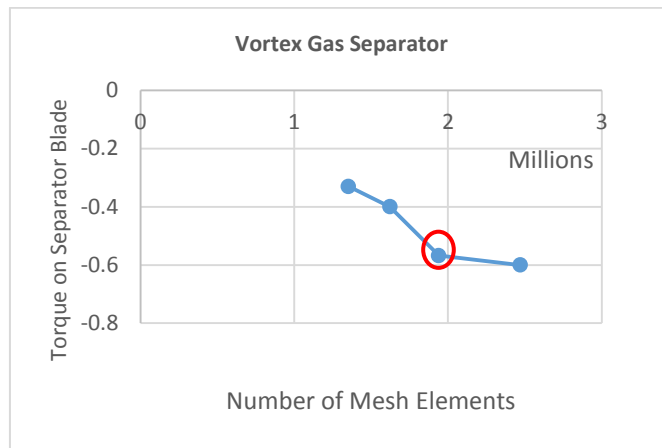
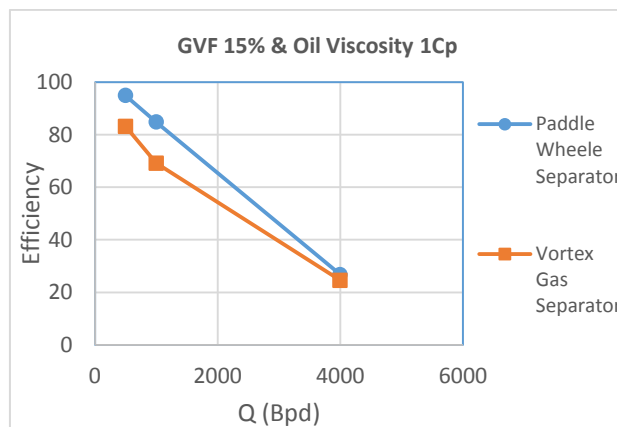


Fig. 8. Vortex grid independency

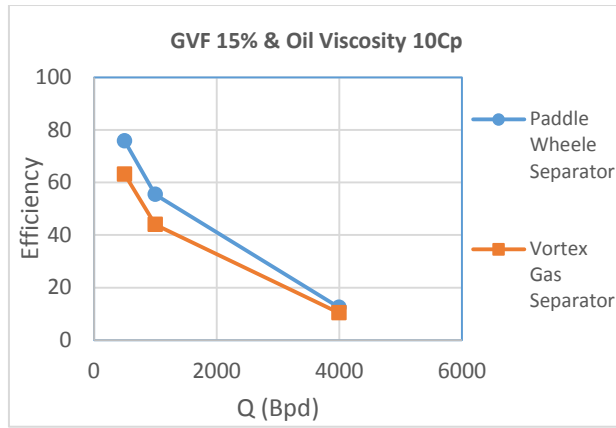
As obtained in results shown in Fig.9, the paddle wheel separator generally shows a better performance in comparison to vortex gas separator. The efficiency of separation decreased significantly with increase in viscosity of liquid flowing into the RGS. However, the performance of the paddle wheel separator is highly affected by viscosity increase rather than vortex gas separator.

The effect of GVF increase on the

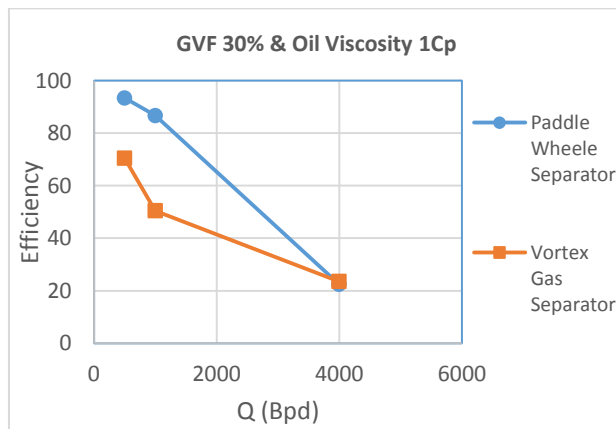
performance of each separator is also observed in this study. It is shown that the Paddle wheel separator is more sensitive to GVF increase in high viscosities, but the reverse is the case for the vortex gas separator in which the separation efficiency is more sensitive to GVF of liquid stream in lower viscosities. However, as the GVF increases, the efficiency of separation in both geometries decreased (Fig. 9).



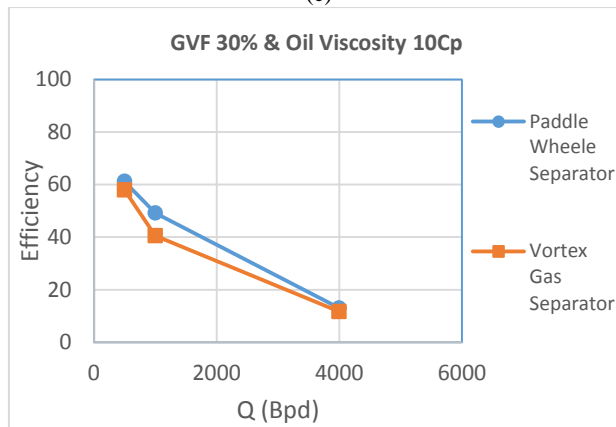
(a)



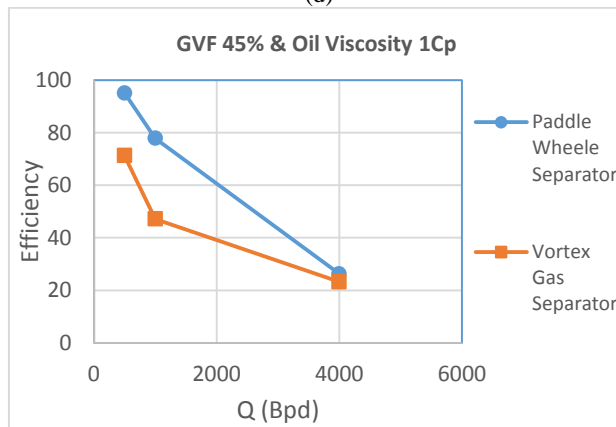
(b)



(c)



(d)



(e)

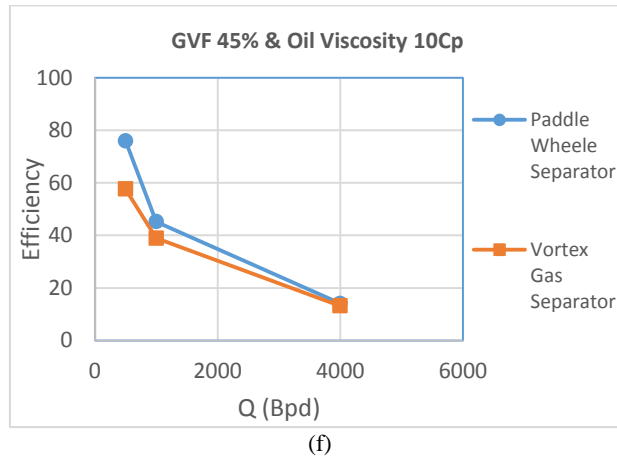
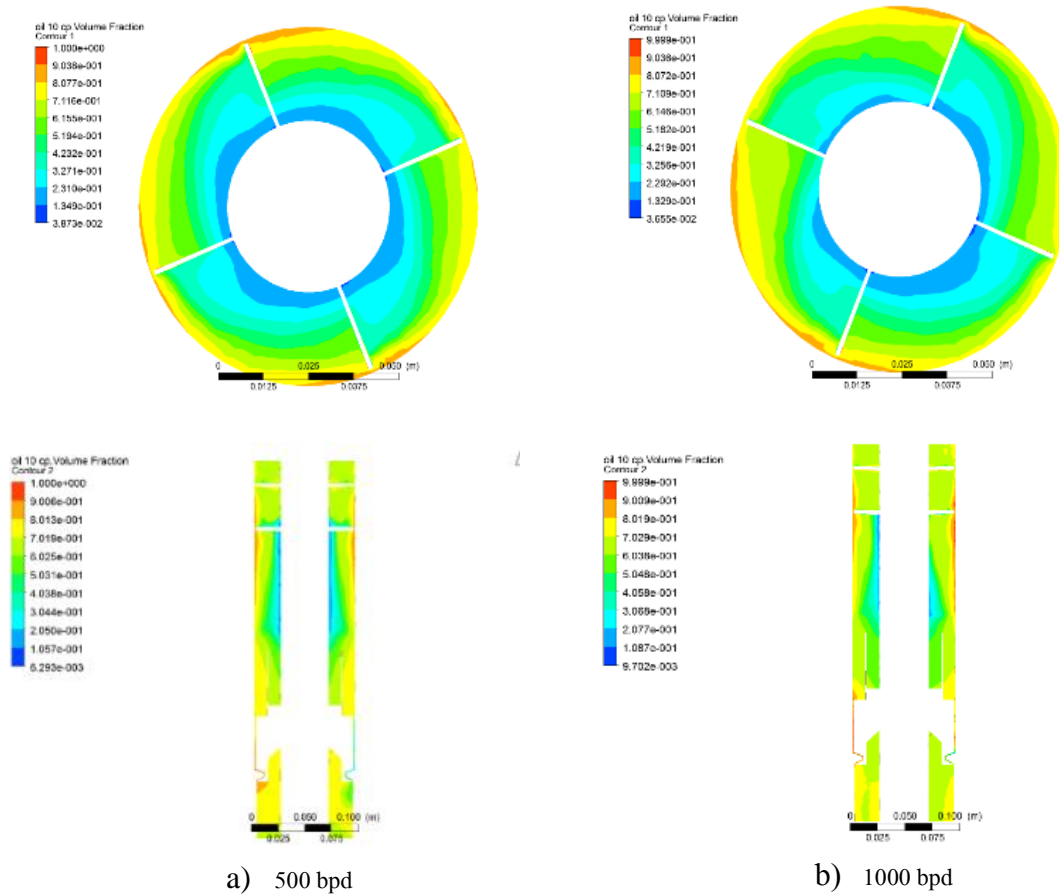


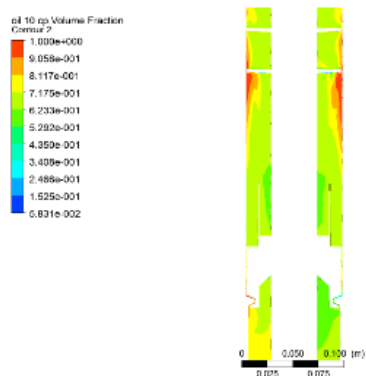
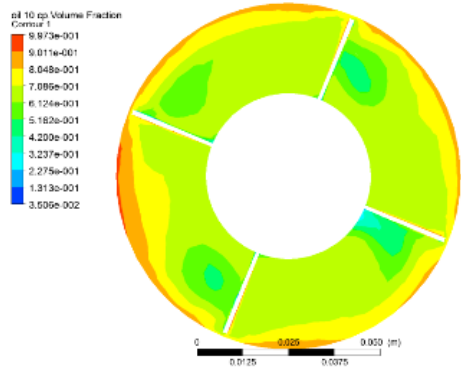
Fig. 9. Effect of GVF and viscosity of paddle wheel and vortex gas separator

- GVF contours

GVF contour for two geometries have been shown in different flow rates and specific inlet GVF and viscosity. The distribution of gas void fraction shows that the concentration of gas in the center part of separation

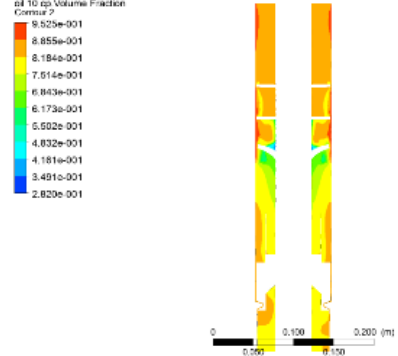
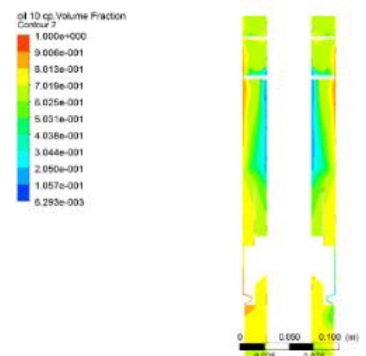
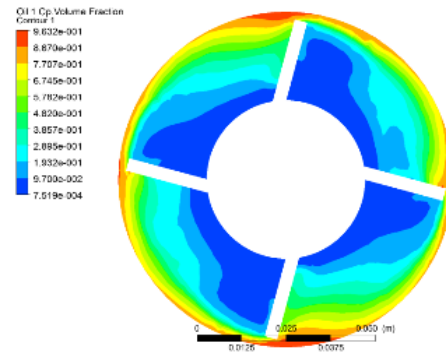
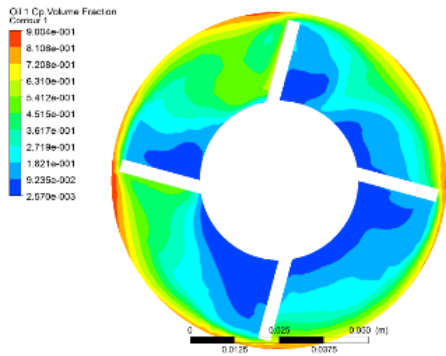
chamber in the paddle wheel type is high. As such, the high efficiencies obtained in this separator type could be attributed to this fact. Also, in higher liquid flow rates, because of the high turbulence effect, gas and liquid phases are mixed together and the efficiency is reduced magnificently (Figs. 10 and 11).





c) 4000 bpd

Fig. 10. GVF contour for paddle wheel separator (viscosity: 10 cp, GVF: 30%)



a) 500 bpd

b) 1000 bpd

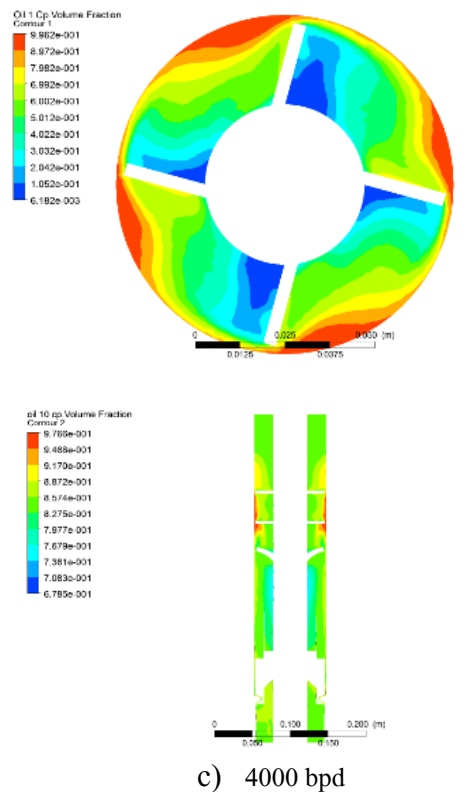


Fig. 11. GVF contour for vortex separator (viscosity: 10 cp, GVF: 30%)

5. Conclusion

- In general, a paddle wheel separator shows better performance in comparison to a vortex gas separator.
- In a paddle wheel separator, the efficiency decreases significantly with increase in viscosity. Also, the same trend happened with increase in gas void fraction.
- In higher viscosities, the decrease in efficiency with increase in void fraction is high in the paddle wheel separator. The opposite happens with vortex gas separator and this trend occurs in lower liquid viscosities.
- Moreover, the concentration of gas in the center area of the separation chamber in the paddle wheel separator is higher than the vortex gas separator, resulting in higher performance of the paddle wheel separator.
- In high flow rates, the turbulence mixes the liquid and gas phases, thereby resulting in poor performance. Also, in higher flow rates, the retention time in the separation chamber is low, and as such, higher separation efficiencies are obtained in lower flow rates.

References

- [1] Zhongyi, W., Changlong Y., Jia H., Yunliang Y., The Analysis of Internal Flow Field in Oil-Gas Separator, *Procedia Engineering* 15, (2011).
- [2] Michael J. Economides, A. Daniel Hill, Christine Ehlig-Economides, *Petroleum Production Systems*, Prentice Hall, PTR, New Jersey, (1993).
- [3] Takacs G., *Electrical Submersible Pumps Manual: Design, Operations, and Maintenance*: Access online via Elsevier, (2009).
- [4] Herl S., Eudey D., *Electric Submersible Pumps Fine Tuned for Gassy Wells*, Schlumberger and Chesapeake Energy, Technology Report, June 15, (2009).
- [5] Liu H., Guo Q., Hu P., *Domestic and overseas Liquid-Liquid Hydro Cyclone Separator Research, Drilling and Production Technology*, (2007).
- [6] Yuan H., *Separate Project*, Beijing, China Petrification Press, (2002).
- [7] Zhongyi, W., Changlong Y., Jia H., Yunliang Y., The Analysis of Internal Flow Field in Oil-Gas Separator, *Procedia Engineering* 15, (2011).
- [8] Alhanati F. J. S., Doty D. R., Schmit Z., *A Simple Model for the Efficiency of Rotary Separators*, *SPE Production and*

- Operation Conference, Technology Report, 28 September (1994).
- [9] Harun A. F., Prado M. G., Shirazi S. A., An Improved Model for Predicting Separation Efficiency of a Rotary Gas Separator in ESP Systems, University of Tulsa and Society of Petroleum Engineering, (2002).
- [10] Lackner G., Alhanati F. J. S., Shirazi S. A., Numerical Simulation of Gas-Liquid Flow in a Rotary Gas Separator, University of Tulsa, (1998).
- [11] Lackner G., The Effect of Viscosity on Downhole Gas Separation in a Rotary Gas Separator, University of Tulsa, (1997).
- [12] Harun A. F., Prado M. G., Doty D. R., Design Optimization of Rotary Gas Separator in ESP Systems, University of Tulsa and Society of Petroleum Engineering, (2003).
- [13] Alhanati F. J. S., Doty D. R., Schmit Z., A Simple Model for the Efficiency of Rotary Separators, SPE Production and Operation Conference, Technology Report, 28 September (1994).
- [14] Maier W., Chochua G., Biba Y., Development of a Rotating Centrifugal Separator Technology for Centrifugal Compressor, GT2010-22222, United Kingdom, Proceedings of ASME Turbo Export 2010, Glasgow.